Petroleum Science 20 (2023) 1584–1597

Contents lists available at ScienceDirect

Petroleum Science

journal homepage: www.keaipublishing.com/en/journals/petroleum-science

Original Paper

2D Janus polymer nanosheets for enhancing oil recovery: From material preparation to property evaluation

Hao Shen [a, 1], Zi-Hao Yang [a, *, 1], Guan-Zhong Wang [a], Yi-Lin Xiong [a, b], Qi-Chao Lv [a], Qi Cao [c], Qi-Qi Niu [a], Yi-Bo Wang [a], Zhao-Xia Dong [a, d, **]

[a] Unconventional Petroleum Research Institute, China University of Petroleum (Beijing), Beijing, 102249, China
[b] Sinopec Zhenhai Refining and Chemical Company, Ningbo, 315207, Zhejiang, China
[c] Shenzhen Institute of Advanced Technology, Chinese Academy of Sciences, Shenzhen, 518055, Guangdong, China
[d] School of Energy Resources, China University of Geosciences (Beijing), Beijing, 100083, China

ARTICLE INFO

Article history:
Received 27 September 2022
Received in revised form
8 December 2022
Accepted 8 December 2022
Available online 9 December 2022

Edited by Yan-Hua Sun

Keywords:
2D materials
Polymer nanosheets
Enhance oil recovery
Janus nature
Amphiphilic property

ABSTRACT

Janus amphiphilic polymer nanosheets (JAPNs) with anisotropic morphology and distinctive performance have aroused widespread interest. However, due to the difficulty in synthesis and poor dispersion stability, JAPNs have been scarcely reported in the field of enhancing oil recovery (EOR). Herein, a kind of organic-based flexible JAPNs was prepared by paraffin emulsion methods. The lateral sizes of JAPNs were ranging from hundreds of nanometers to several micrometers and the thickness was about 3 nm. The organic-based nanosheets were equipped with remarkably flexible structures, which could improve their injection performance. The dispersion and interfacial properties of JAPNs were studied systematically. By modification of crosslinking agent containing multiple amino groups, the JAPNs had excellent hydrophilicity and salt resistance compared with conventional inorganic or composite nanosheets. The settling time of nanosuspension with NaCl and $CaCl_2$ at a low salinity of 1000 mg/L was over 240 h. The value could also remain 124 h under the salinity of 10,000 mg/L NaCl. With the dual functionalities of Janus amphiphilic nature and nanoparticles' Pickering effect, JAPNs could change rock wettability and form emulsions as "colloidal surfactants". In particular, a new technology called optical microrheology was pioneered to explore the destabilization state of nanosuspensions for the first time. Since precipitation lagged behind aggregation, especially for stable suspension systems, the onset of the unstable behavior was difficult to be detected by conventional methods, which should be the indicator of reduced effectiveness for nanofluid products. In addition, the oil displacement experiments demonstrated that the JAPNs could enhance oil recovery by 17.14% under an ultra-low concentration of 0.005% and were more suitable for low permeability cores. The findings can help for a better understanding of the material preparation of polymer nanosheets. We also hope that this study could shed more light on the nanoflooding technology for EOR.

1. Introduction

The development of nanotechnology has provided infinite possibilities for the energy and fuel industries (Lv et al., 2022; Olayiwola and Dejam, 2021; Qu et al., 2022a, 2022b). Nanofluid flooding, a new displacement technology, has attracted more and more attention from researchers all over the world in recent years (Xue et al., 2014; Yakasai et al., 2021). Nanofluid refers to a colloidal suspension of nanomaterials, whose preparation is affected by many factors, such as temperature, particle size, dispersant type, concentration, solvent pH, ultrasonic time, or stirring speed. Generally, nanomaterials are roughly defined as particles with a grain size of 1–1000 nm. They can also be subdivided into four dimensions with 100 nm as the boundary, including 0D

* Corresponding author. Unconventional Petroleum Research Institute, China University of Petroleum (Beijing), Beijing, 102249, China.
** Corresponding author. Unconventional Petroleum Research Institute, China University of Petroleum (Beijing), Beijing, 102249, China.
E-mail addresses: zihaoyang@cup.edu.cn (Z.-H. Yang), dongzx@cugb.edu.cn (Z.-X. Dong).
[1] These authors contributed equally to this work.

https://doi.org/10.1016/j.petsci.2022.12.005

Nomenclature:

2D	Two dementional
AFM	Atomic force microscopy
AIBN	Azodiisobutyronitrile
AJNs	Amphiphilic Janus nanosheets
DWS	Diffusion wave spectroscopy
EDC	*N*-(3-dimethylaminopropyl)-*N*′-ethylcarbodiimide hydrochloride
EOR	Enhancing oil recovery
FT-IR	Fourier transform infrared spectroscopy
GPC	Gel permeation chromatography
HAADF	High angle annular dark field
HSMA	Hydrolyzed SMA
IFT	Interfacial tension
JAPNs	Janus amphiphilic polymer nanosheets
MA	Maleic anhydride
MCH	Methylcyclohexane
MSD	Mean square displacement
MS-DWS	Multispeckle-DWS
SEM	Scanning electron microscopy
SMA	St-MA copolymer
s-NHS	*N*-hydroxysulfosuccinimide sodium salt
St	Styrene
TEM	Transmission electron microscopy
TEPA	Tetraethylenepentamine
TGA	Thermal gravimetric analysis
TSI	Turbiscan stability index
ΔI_{BS}	Backscattered light intensity
M	Molecular weight
$\overline{M}_n$	Number average molecular weight
P	Polydispersity
ΔT	Transmitted light intensity

nanospheres and nanogranules, 1D nanowires and nanotubes, 2D nanosheets, and 3D nanoblocks (Liang et al., 2022).

Due to the ultra-small physical size, nanoparticles have large specific surface areas, which will generate a huge diffusion drive when dispersed in solvent. Laboratory experiments and field applications have shown that oil recovery can be enhanced by injecting high-performance nanofluids. The displacement mechanism of nanofluids can be summarized into five aspects: (1) Forming into a molecular deposition film and generating structural partial pressure. Due to Brownian motion and electrostatic force, nanoparticles will self-assemble into a wedge structure in the three-phase region of water–oil–rock, which will produce a forward thrust on crude oil (Wasan and Nikolov, 2003). (2) When nanomaterials are deposited and plugged in small pores of the formation, sweep volume will be increased accordingly. The nanofluids will function as plugging agents for low permeability pores. (3) Due to the high specific surface area and surface energy, nanoparticles are prone to absorb on the rock surface, changing the wettability and detaching oil off the rock (Wasan and Nikolov, 2003). (4) When encountering heavy oil molecules, nanoparticles can reduce the flocculation of asphaltene and slow down its sedimentation (Ke et al., 2022). (5) If nanoparticles are equipped with Janus nature and amphiphilic property, they will be able to reduce interface tension (IFT) and the interface adsorption capacity will be greatly improved accordingly (Walther and Müller, 2008). With the help of flooding turbulence in the pores, nanofluids can mix with oil to form Pickering emulsions (Liang et al., 2018). A great number of nanoparticles have been reported in recent years, however, the results collectively demonstrate that they did not enhance oil recovery as much as researchers have expected (Liang et al., 2022; Rezk and Allam, 2019). It can be ascribed to the fact that nanoparticles are far outsize common surfactant molecules, and their interfacial adsorption capacities are reduced considerably. The shapes of nanoparticles also have a great influence on their interface properties. Compared with spherical, rod-shaped, or other irregular shapes, the rotation of nanosheets at the interface is more restricted (Tan et al., 2017). By endowing different hydrophilic and hydrophobic groups on the opposite sides, nanosheets will exhibit Janus nature and amphiphilic properties, which makes the orientation of their two sides more directional. The colloidal dispersion and interfacial adsorption of nanosheets may also be artificially regulated. It is expected to bring innovation to the development of nanoflooding technology.

Based on the chemical composition, nanosheets can be classified into three categories: inorganic nanosheets (Liang et al., 2011), polymer/inorganic composite nanosheets (Chen et al., 2012), and polymer nanosheets (Liu et al., 2017; Zeng et al., 2022). Inorganic nanosheets are often equipped with abundant optical, electrical, magnetic, or other functions. The mechanical and thermal stabilities are also strengthened by their compact structures. However, the chemical groups on the surface are monotonous, which limits the environmental adaptability of inorganic nanosheets. SiO_2-based nanosheets are the most commonly used and cost-effective nanoparticles (Yin et al., 2019c). However, the chemical composition drives them to adsorb and agglomerate together rapidly in aqueous solution. The high-salt and high-temperature environment will further promote the instability of nanosuspensions, which may cause serious reservoir damage. In addition to the mechanical and thermal stabilities, the properties of composite nanosheets can be improved by grafting polymer segments on the surface (Percebom and Costa, 2019). The disadvantage is that their synthesis relies on the template basis of inorganic nanosheets, which greatly reduces the selectivity of graft polymerization. Polymer nanosheets have superior aggregation behavior and flexible framework, which gives them better injectability and passability in low permeability formations. By regulating the original monomers and the subsequent grafting processes, the physicochemical properties of polymer nanosheets can be easily adjusted. Compared with inorganic nanosheets, there are more covalent grafting sites on polymer nanosheets, which are available for functional modification. Considering the complex condition in oil fields, especially the high salt and low permeability reservoirs, the 2D Janus polymer nanosheets with artificial modification and flexible structure may hold more potential for further development in EOR processes (Yakasai et al., 2021). The advantages and opportunities of the JAPNs can be summarized into three aspects. (1) Material synthesis: It is easier to design and construct initial polymers or prepolymers. The chemical groups on the surface of nanosheets can be selectively regulated, which is beneficial to improve their structural stability, amphiphilic property, and salt tolerance. (2) Colloidal stability: Common AJNs are prone to disperse unstably in aqueous solution. For example, graphene-based AJNs (aggregation and precipitation within 1 h with 580 mg/L NaCl) (Luo et al., 2017), SiO_2-based AJNs (precipitation within 24 h with 5000 mg/L NaCl) (Yin et al., 2019c), MnS_2-based AJNs (compounding with surfactants to improve the dispersibility) (Qu et al., 2022a, 2022b), and Fe_3O_4-based nanosheets (being greatly affected by gravity and magnetism) (Zhang et al., 2022b).

JAPNs with regulated groups have great potential to ameliorate this problem. (3) Injection performance: Compared with inorganic materials, organic-based JAPNs should possess more flexible structures, which improves their injectivity especially in low permeability reservoirs. The shape transformation enables nanosheets to penetrate deep into the reservoir. After rapid development in recent years, a variety of strategies have been proposed for the synthesis of Janus nanosheets (Zhang et al., 2018). According to the synthesis theories, there are several methods such as surface modification method, interfacial sol-gel method, solvent-induced self-assembly method, template method, intercalation method, stripping method, etc. In terms of synthesis direction, it can be summarized into two categories: top-down method and bottom-up method. The top-down method relies on the pre-synthesized 2D layered nanostructures. It is limited by the incompleteness and irregularity of the surface structure after crushing. The bottom-up method is driven by the reduction of Gibbs free energy, which makes it close to thermodynamic equilibrium. The problem lies in poor synthesis controllability and high production cost. By contrast, bottom-up method has shorter synthesis processes, but limited selection of monomers. Top-down method is supposed to produce more uniform nanosheets.

Compared with well-rounded research of spherical Janus particles and silica-based nanosheets, the research on 2D polymer nanosheets has been scarcely reported. Several challenges remain before these high-performance polymer-based nanosheets can be used in practical field applications (Stupp et al., 1995; Zhan et al., 2022; Zhou et al., 2015): (1) It is difficult to accurately control the direction and degree of polymerization. As the conformation of the polymer is prone to spatial distortion, it tends to obtain hypercrosslinked bulks instead of 2D nanosheets (Peplow, 2016). (2) The nanosheets prepared by conventional methods are not Janus amphiphilic and need further grafting modification, which reduces the yield and structural stability. (3) Most synthesis processes are complicated and costly, which is not conducive to large-scale production. (4) Currently, the synthesis of nanosheets and properties such as optics, electrochemistry, and catalysis occupy the majority of researchers' interests. The colloidal and interfacial properties closely related to the practical application of EOR are far from well understood. Our previous work (Shen et al., 2022; Yin et al., 2019a, 2019b, 2019c, 2020, 2021; Zhang et al., 2022a, 2022b) has presented many kinds of amphiphilic Janus nanosheets (AJNs) and various performances, the application of 2D Janus polymer nanosheets for enhancing oil recovery has not been reported as far as we know.

The dispersion stability in aqueous solution plays a prerequisite role for nanosheets to be prepared into homogeneous nanofluids and penetrate deeply into the reservoir. Even though some degree of aggregation has occurred inside the nanosuspensions with relatively good stability, there may still be little sedimentation deposited over a long time. The precipitation of suspension systems lags behind aggregation, and the better the stability, the longer the lag time. The decrease in effectiveness of nanofluid products begins with nanosheets gradually losing their independent dispersion forms rather than the appearance of precipitation. However, most traditional methods rely on the thickness of the precipitate or altered light transmittance due to settling. It is necessary to develop new techniques to accurately determine the start time of instability stats for nanofluids.

At present, the research of 2D Janus polymer nanosheets is still in its infant stage. The lack of systematic research on the material preparation and property optimization of JAPNs, especially the weak stability of nanosheets in brine, hinders their wide application. In this paper, the material preparation, property evaluation, and EOR capacity had been studied systematically. A general sketch is shown in Fig. 1. First, the pre-synthesis amphiphilic copolymer was restrained to the paraffin/water interface. Then the processes of activation, polymerization, enucleation, and crushing were carried out in sequence. Thereby, a type of JAPNs was constructed based on paraffin templates, which was a common thermal phase change material. The dispersion stability and salt resistance of the JAPNs nanofluid were significantly improved by introducing multiple amino groups through amidation. Systematic research, including chemical composition, microstructure observation, dispersion stability, and interfacial adsorption of JAPNs has been carried out. Moreover, the EOR ability of 2D Janus polymer nanosheets was investigated for the first time. We hope that this paper can provide scientific guidance for the synthesis, analysis, and application of polymer nanosheets.

2. Experimental

2.1. Materials

Maleic anhydride (MA) was stored in a vacuum-drying oven to prevent it from deliquescing with water in the air. Styrene (St) was purified by filtering through an Al_2O_3-filled column and then preserved at −18 °C to prevent premature self-aggregation. Anhydrous $CaCl_2$ particles were put into toluene bottles to absorb trace water. Azodiisobutyronitrile (AIBN) was also kept at low temperatures. Other chemical materials, including NaOH, *N*-hydroxysulfosuccinimide sodium salt (s-NHS), *N*-(3-dimethylaminopropyl)-*N*′-ethylcarbodiimide hydrochloride (EDC), tetraethylenepentamine (TEPA), and methylcyclohexane were commercially available and used as received without further purification. The crude oil was mined from Tarim Oilfield in China, whose viscosity was 10.9 mPa s (25 °C, 0.1 MPa). The salinity of the simulated formation water was 10,000 mg/L, including NaCl (9000 mg/L) and $CaCl_2$ (1000 mg/L).

2.2. Preparation

Copolymerization: St (0.12 mol) and MA (0.12 mol) were dissolved in 300 mL toluene. N_2 was introduced into the system for

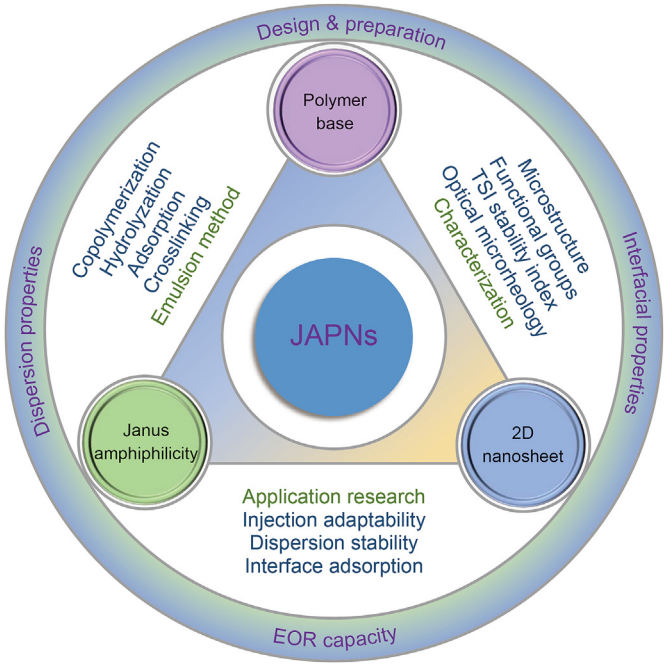

Fig. 1. General sketch of main research contents.

30 min. Then the solution was heated at 85 °C for 8 h with reflux and stirring. After cooling down, the suspension was vacuum filtered and washed twice with toluene. The insoluble substance (SMA) would be dry in an oven.

Hydrolyzation: The SMA copolymer was put into 9 times the water. NaOH was used to adjust the alkali of the solution. The mixer was stirred at 80 °C for more than 3 h. The obtained 10 wt% hydrolyzed SMA (HSMA) solution would be stored in an opaque bottle.

Adsorption: HSMA solution (10 g), water (90 g), and paraffin (10 g) with a melting point of 52–53 °C were added into a glass bottle and heated to 70 °C, and then emulsified for 5 min under 15,000 rpm by an emulsifier homogenizer. After cooling down in an ice bath, the mixture was separated by centrifugation.

Crosslinking: The adsorbed paraffin was dispersed in water (100 g) again. EDC (0.5 g) and s-NHS (0.5 g) were added to activate the carboxyl groups for 30 min. The pH of the solution was adjusted to be neutral. Then tetraethylenepentamine (3 mL) was put into the mixture and shaken for 12 h. The paraffin cores were removed by methylcyclohexane and washed 3 times. After being ultrasonic by a high-power cell ultrasonic pulverizer, the 2D JAPNs would be synthesized eventually. The schematic of preparation is shown in Fig. 2.

2.3. Characterization

Gel permeation chromatography (GPC, PL-GPC 220) was used to determine the composition distribution and molecular weight distribution of the copolymer. Thermal gravimetric analysis (TGA, TA Instruments SDT Q600) was conducted to analyze the relationship between weight-related quantities (such as mass, solid residue, or residue rate.) of the sample and the temperature. Fourier transform infrared spectroscopy (FT-IR, Bio-Rad Laboratories FTS-6000) was used to measure the chemical groups or compositions. Emulsifier homogenizer (IKA ULTRA-TURRAX T18 Basic) was used to stir the mixed solution at high speed. High-power cell ultrasonic pulverizer (Scientz-IID) was employed to crush crosslinked polymer films. The microstructure observations were conducted by scanning electron microscopy (SEM; FEI Quanta 200), transmission electron microscopy (TEM, FEI Talos f200s), and atomic force microscopy (AFM, Bruker Dimension Edge). The muti-system equipment (Teclis Scientific TrackerTM Interfacial Rheometer) was used to study the contact angle and interfacial tension. Ultraviolet–visible spectrophotometer (Unico UV4802S) was used to research the transmissivity of JPN/water suspension with time. Multiple lights scattering experiments were performed by Turbiscan (Formulaction Turbiscan Lab) to quantitatively calculated the dynamic data in settlement processes. Particularly, a new measuring technology based on Rheolaser optical microrheometer (Formulation Rheolaser Master) is proposed to investigate the microscopic dispersion condition of the nanosuspension systems.

2.4. EOR experiments

A core displacement device was set up to investigate the injection performance and EOR capacity of JAPNs nanofluids (Fig. 3). Artificial homogeneous cores were used to explore the compatibility of nanosheets in reservoir rocks. The cores were 7 cm long and 2.5 cm in diameter. All experiments were carried out at room temperature. The pressure data were recorded instantaneously by pressure sensors connected to a computer. The main experimental process was as follows: (1) The pore volume and permeability of the cores were tested in advance with deionized water. (2) The water-bearing cores were re-dried and saturated with oil by vacuuming. (3) The flow rate of primary water flooding was 0.2 mL/min and was injected until no more oil come out from the tail end. (4) 2 PV nanofluids of 0.005% JAPNs were injected at 0.2 mL/min during the nanofluid flooding. (5) The secondary water flooding was carried out under the same conditions as the previous experiments. Throughout the process, the oil output from the end of the core holder was collected and recorded to calculate the recovery factor.

3. Results and discussion

3.1. Material preparation

Compared with other types of nanosheets, it is more convenient to introduce functional groups into polymer nanosheets by selectively adjusting the composition of monomers. Hydrophilic MA and hydrophobic St, which both contain polymerizable C=C bonds, were selected to be the initial monomers. As a strong electron-absorbing substance, MA is inclined to alternate copolymerize with styrene derivatives with almost no self-aggregation. The electron-donating monomer, styrene, is the simplest member of unsaturated aromatic hydrocarbons. Nearly 80% of functional polymer materials are made of polystyrene (Scheirs and Priddy, 2003). The preparation of SMA followed precipitation

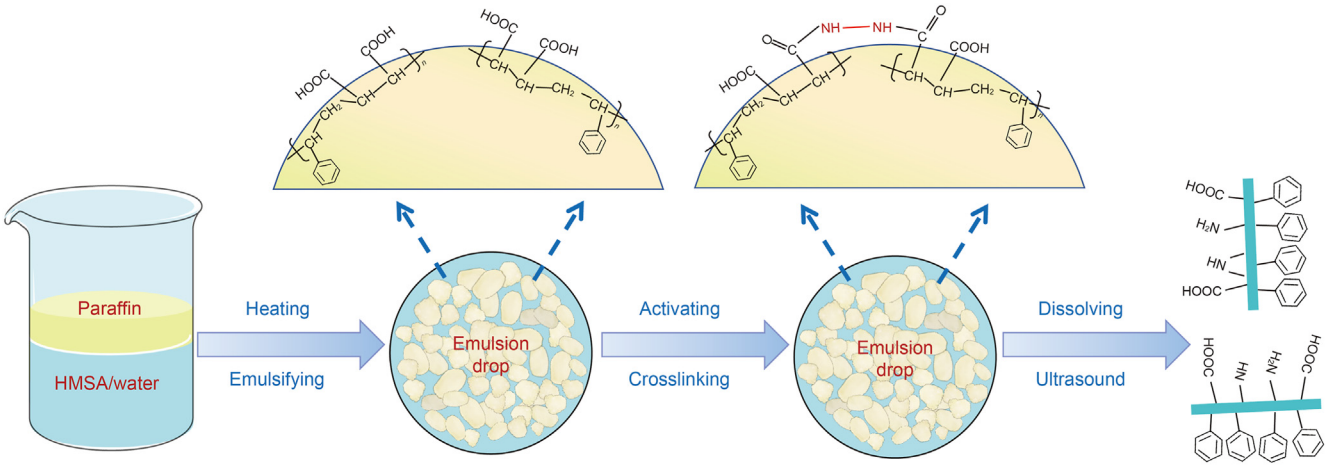

Fig. 2. Schematic of preparation of JAPNs via paraffin templates.

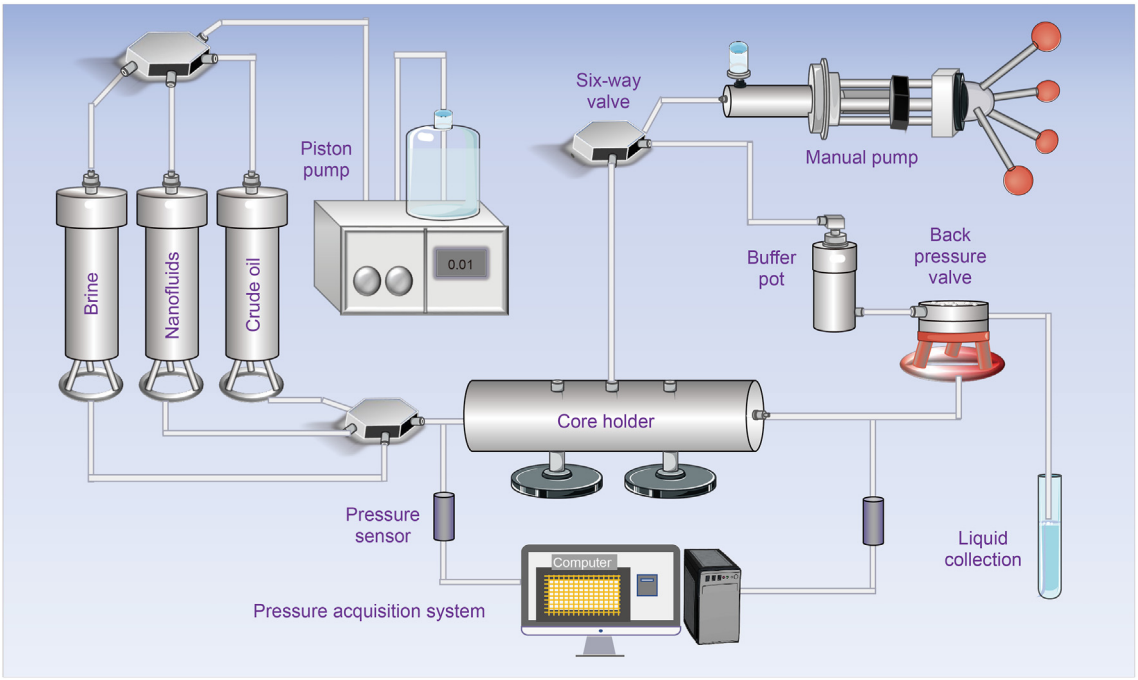

Fig. 3. Schematic diagram of the core displacement device.

polymerization, in which the reactants are soluble in the solvent while the products are not. The molecular weights of SMA turned out to be 18,019 Da and the distribution rate was 1.47 (Fig. 4a). Inefficient control during the accelerated exothermic period would deteriorate the molecular weight distribution, which may affect the regularity of amphiphilic copolymers during interfacial adsorption. After reacting with heated alkaline water, anhydride would be hydrolyzed into dicarboxylic acid, and hydrophobic SMA was converted into amphiphilic HSMA.

From a molecular point of view, HSMA could present a typical Janus structure when self-assembling on the oil-water interface. After the liquid paraffin particles had been cooled to the solid state (Fig. 4b), the groups' orientation would also be confined, with hydrophilic carboxyl groups facing the aqueous phase and hydrophobic benzene rings fixed in the paraffin wax (Jin et al., 2008). The amidation reaction was an effective path for connecting carboxyl and amino groups under a mild reaction condition. HSMA polymers were connected from 1D lines to 2D networks by the long chain amino crosslinker. After dissolving and ultrasound, 2D Janus polymer nanosheets with amphiphilic nature would be prepared eventually.

3.2. Preliminary characterization

Physical structure (shape and size) is one of the most fundamental properties of 2D nanosheets. Fig. 5a and b presented SEM images of scattered and stacked JAPNs, most of which had particle sizes ranging from hundreds of nanometers to several micrometers. One interesting finding was that there was a rare-shaped nanosheet in Fig. 5a, which looked like a curled handkerchief or tissue. The ability to curl both sides at the same time confirmed that JAPNs were equipped with remarkably flexible structures, which was

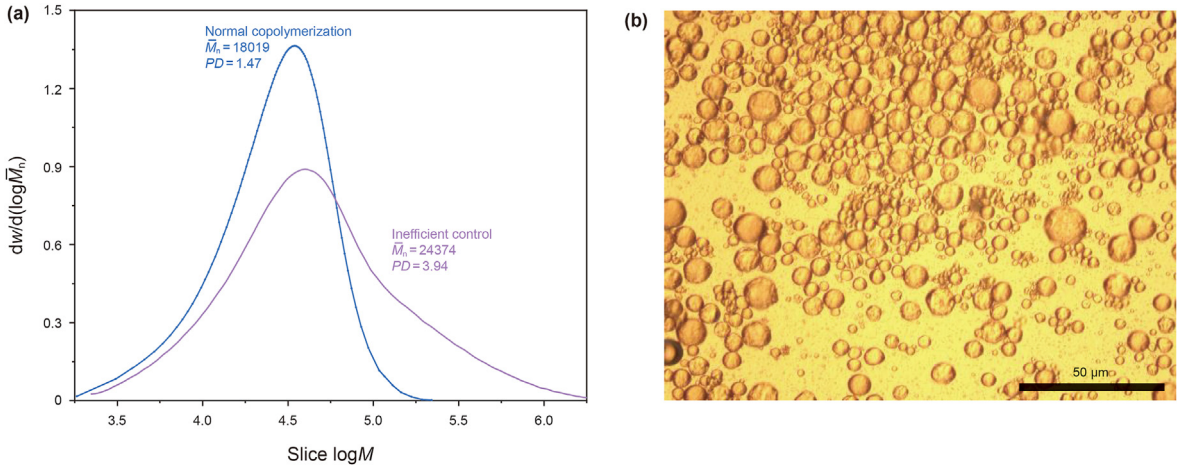

Fig. 4. (**a**) Gel permeation chromatography; (**b**) Optical image of paraffin generated by emulsifier homogenizer.

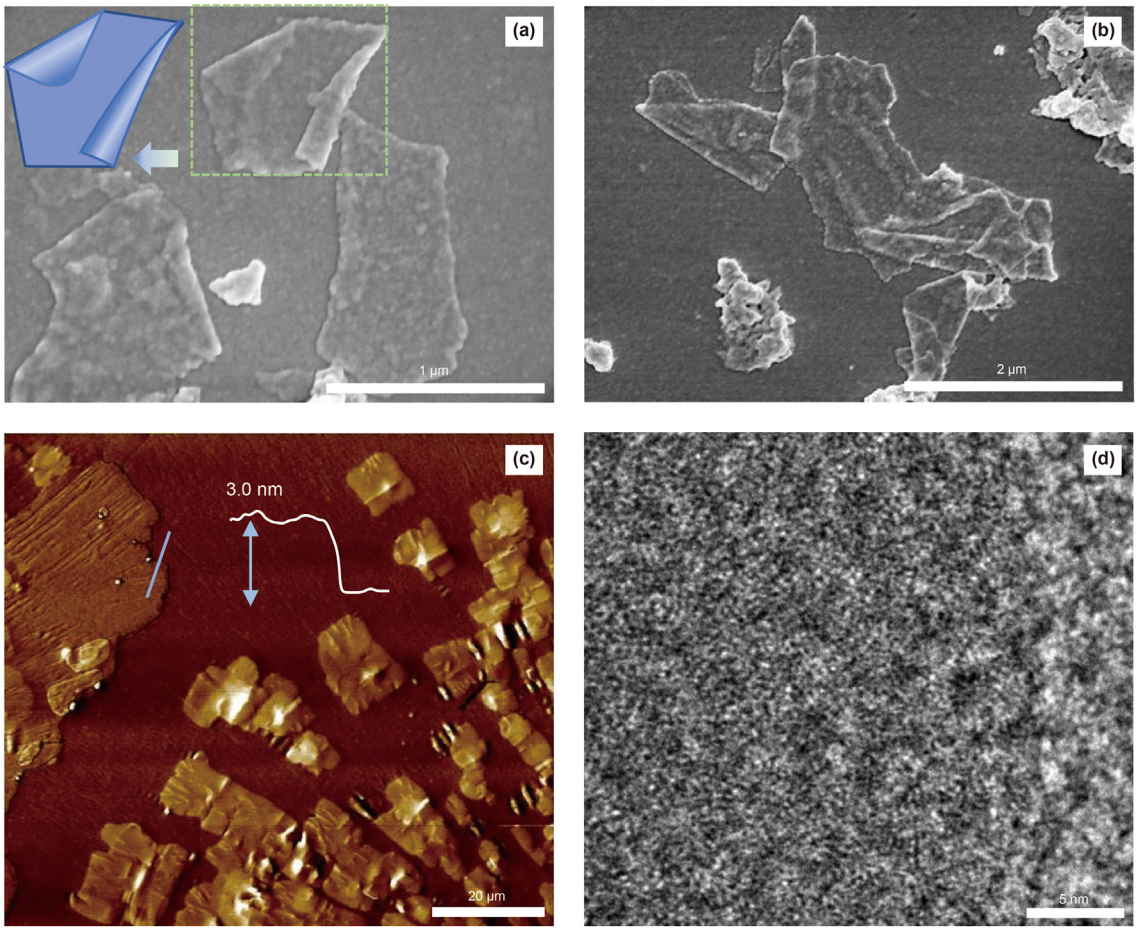

Fig. 5. SEM images of **(a)** scattered and **(b)** stacked nanosheets; **(c)** AFM and **(d)** high-resolution TEM image of JAPNs.

beneficial to improve the injection performance of nanofluids. The results may be explained by the fact that the bond energy of polymers was relatively weak, and thereby, the chain nodes could vibrate and rotate internally during molecular thermal movement (Mu et al., 2015). The nanosheets in Fig. 5b were not rigidly stacked together but appeared to fold like gauze, which was also a side indication of the thinness of JAPNs. The accurate thickness was about 3 nm (Fig. 5c). As shown in the high-resolution photographs of TEM in Fig. 5d, the constituent atoms on the surface of the nanosheets were non-periodically arranged, and there were no lattice stripes. It was concluded that the JAPNs were obtained with amorphous non-crystalline solid structures. The high angle annular dark field image (HAADF) (Fig. 6) proved that the crushed nanosheets had irregular structures. The elements of C and N are uniformly distributed on the surface of JAPNs while the O element has less residue.

Chemical compositions of SMA, HSMA, and JAPNs were investigated by FI-IR spectra (Fig. 7a). For the results of SMA, the absorption peaks at 1855 and 1780 cm^{-1} belonged to C═O in acid anhydride. The peak at 1225 cm^{-1} indicated the presence of C–O–C in cyclic anhydride. Peaks at 1454, 1495, and 1632 cm^{-1} were attributed to the vibration absorption of C═C in benzene rings. As for HSMA, the peaks belonging to C═O were replaced by carboxyl groups in 1710 cm^{-1}. The hydroxyl peak obtained by hydrolysis appeared at 3450 cm^{-1}. For the JAPNs data, peaks at 1705 and 3450 cm^{-1} were ascribed to the residual carboxyl groups. Meanwhile, the peaks of amide groups gave prominence in the infrared spectrum. Peaks at 1640 cm^{-1} indicated the stretching vibration absorption of C═O in amide groups, which was also called the amide I region. The typical amide II region of bending vibration peak of N–H was located in 1565 cm^{-1}. The clear cleavage of these two regions was an important indication that the JAPNs products contained plentiful secondary amides rather than primary amides since these two regions would overlap in primary amides. Tertiary amides should not be considered because they have no N–H peaks at all. The peak at 700 cm^{-1} was attributed to the bending vibration absorption of N–H and the peak at 1400 cm^{-1} indicated the presence of C–N. Fig. 7b shows the TGA curves of SMA and JAPNs. Both samples underwent severe weight reduction between 300 and 450 °C, which could be attributed to the disintegration of the carbon chains on the polymer framework. However, JAPNs displayed an additional weight loss stage between 180 and 300 °C. This discrepancy may be caused by the decomposition of the amide groups to produce ammonia and water. With benzene rings and heterocyclic structures containing anhydride, SMA was more thermally stable before 360 °C. The high residual value of HSMA was mainly due to NaCl impurity produced during pH adjustment, whose boiling point is as high as 1464 °C. The results demonstrated the chemical changes of various products during the synthesis process and the preliminary characterization above can verify that 2D Janus polymer nanosheets were prepared through the paraffin template method.

3.3. Dispersion properties

Due to the huge specific surface area, nanoparticles tend to

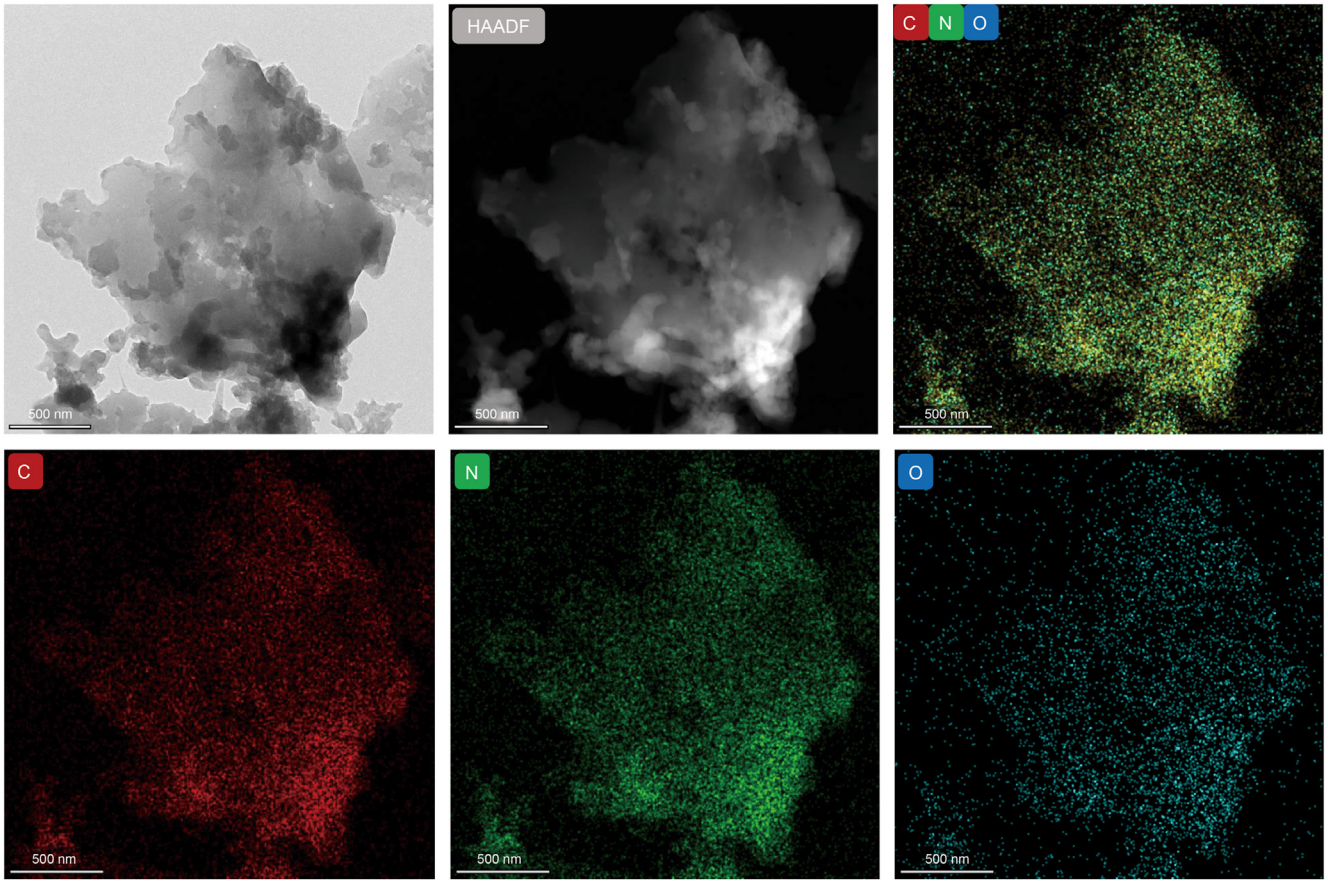

Fig. 6. HAADF images of JAPNs.

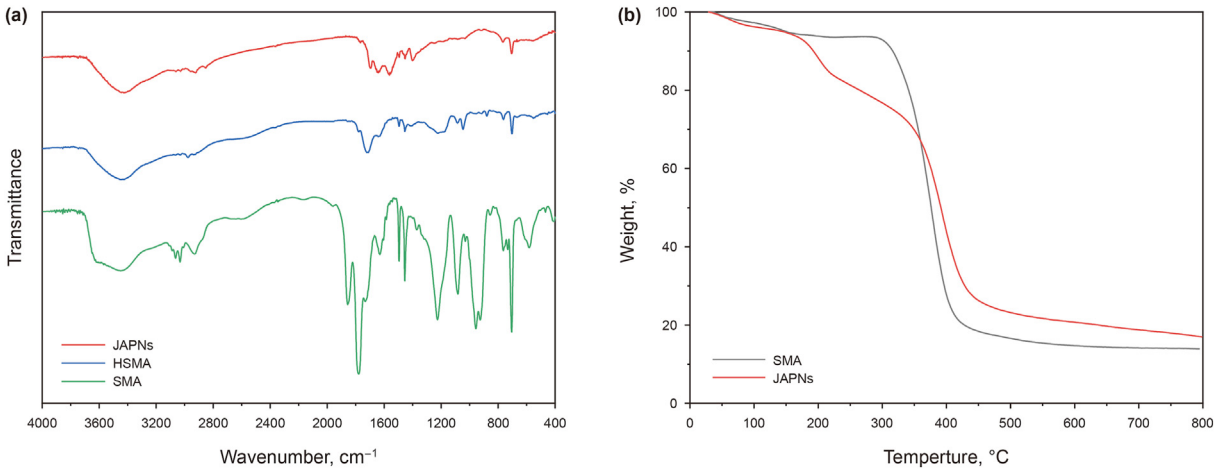

Fig. 7. (**a**) FI-IR spectra of SMA, HSMA, and JAPNs; (**b**) TGA of SMA and JAPNs.

aggregate spontaneously to reduce their surface energy. Dispersion instability will make it difficult for nanofluids to penetrate into the reservoir and settle in advance (Hua et al., 2015). Therefore, systematic research on the dispersion stability of nanosheet suspension systems is extremely important.

3.3.1. Settlement experiments

Fig. 8a shows the dispersion states of JAPNs in various solvents, including methylcyclohexane (MCH), xylene, toluene, ethanol, and water. The good dispersion of a certain mass (0.1 wt%) of nanosheets in different polar solvents indicated that JAPNs were amphiphilic. Fig. 8b and c present the sedimentation observation of JAPNs in water with different pHs. After 24 h at room temperature, the dispersion situation of pH = 1 had changed dramatically. Some white precipitate appeared at the bottom. There were also some unstable aggregations in the sample of pH = 13. However, the causes of these two suspensions should be different. In acidic conditions, the COO^- groups on the hydrophilic side of nanosheets

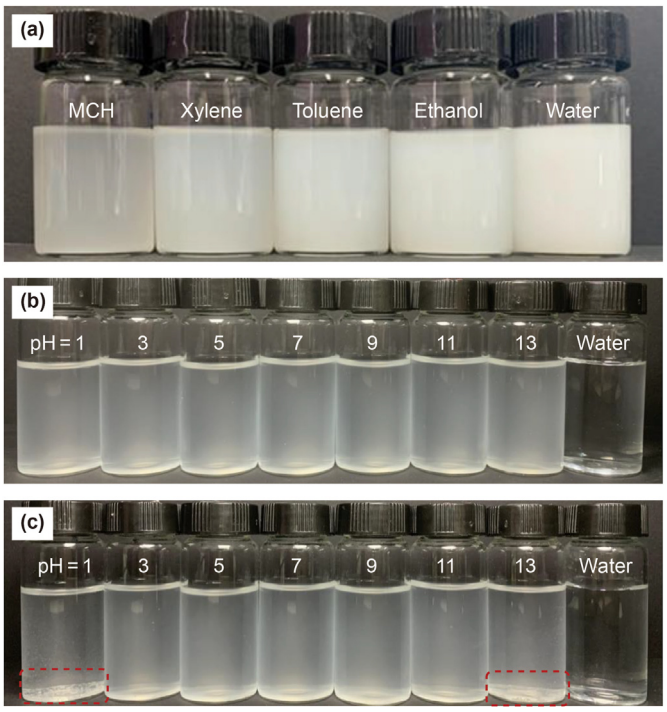

Fig. 8. (**a**) Dispersion states of JAPNs (0.1%) in different polar solvents; Dispersion states of JAPNs (0.005%) in water with different pH **(b)** at the beginning and **(c)** after 24 h.

would protonate with H^+, thereby, reducing the affinity of JAPNs with water. As for pH = 13, the secondary amine groups with weak alkaline would be the main factor affected. There was almost no difference by visual observation for the other 5 samples after 24 h. The JAPNs suspensions could remain stable under a relatively mild pH condition.

Light transmittance experiments were used to digitally record the transparency differences of nanofluid with time. Three concentrations (0.001%, 0.005%, 0.025% of JAPNs) and three salinities (1000 mg/L NaCl, 1000 mg/L $CaCl_2$, 10,000 mg/L NaCl with 0.025% JAPNs) of nanofluids were conducted for their transmittance (Fig. 9). For the sample with the lowest concentration, the transmittance of 0.001% got to 84.6% at the beginning and then increased to 90% after 48 h. In order to fairly estimate the final settling time of nanosuspension, the transmittance of 0.001% at 24 h, which turned out to be 88%, was selected as the endpoint value. It was worth noting that there were still a small number of dispersed nanosheets that remained in the solvent at this transmittance. The results showed that JAPNs nanofluids exhibited excellent dispersion stability, the longest settling time could be delayed to 480 h. The presence of salt especially high mineralization would accelerate the aggregation process. Exacerbate the trend. It was believed that the double electric layer on the particle surface would be compressed by the cations in the water, resulting in a lower energy barrier to prevent aggregation. Additionally, divalent cations had higher charge densities per unit area compared to monovalent cations, and the ability to reduce the colloidal energy barrier was also stronger (Yin et al., 2019a). However, the settling time of samples with NaCl and $CaCl_2$ at a low salinity of 1000 mg/L was over 240 h. The value also reached 124 h even under the salinity of 10,000 mg/L NaCl. The stabilization may be benefitted from the plentiful hydrophilic groups on the surface of JAPNs. During the crosslinking process, a large number of secondary amino groups were introduced into the nanosheets, while the carboxyl groups sensitive to salt were

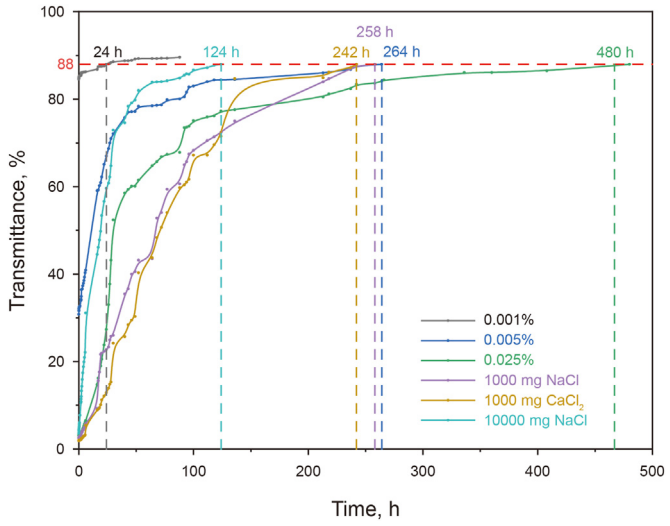

Fig. 9. The transmittance changes of nanosuspensions with different concentrations and salinity.

partially replaced by amide groups (Qu et al., 2020; Luo et al., 2018, 2019). In addition to electrostatic repulsion and solvation strengthened by hydrophilic groups, branched chains on the polymer framework would also retard the aggregation rate between nanoparticles (Mcclements, 2005; Haruna and Wen, 2019). Compared with other types of AJNs, the polymer-based AJNs reported in this paper showed excellent colloidal stability and salt resistance. Furthermore, the carboxyl and amino groups on the surface of the nanosheets also provide more possibilities for further grafting modification. In summary, self-stabilized polymer nanosheets with no extra stabilizer suggested better suitability for oilfield applications.

3.3.2. Turbiscan measurement

To further characterize the aggregation process and settlement dynamics of JAPNs, Turbiscan was employed to measure the suspension information through the intensity changes of transmitted and backscattered light (Xiong et al., 2020). The working principle of the device is shown in Fig. 10a. Since the instrument is based on the principle of diffusion wave spectroscopy (DWS), the sample needs to have certain turbidity. Relatively high concentrations (0.005%, 0.025%, 0.05%, and 0.1%) were used to calculate the Turbiscan stability index (TSI) value of JAPNs. TSI is an index used to describe the dispersion stability of suspension systems. When TSI<1, it means the suspension is extremely stable. When TSI is between 1 and 10, the system is undergoing a transition from uniform to inhomogeneous. When TSI>10, it means the settlement phenomenon has been visible (Li et al., 2017). As shown in Fig. 10b, the growth rate of TSI was inversely proportional to the concentration of JAPNs, which was consistent with the transmittance experiment. This was partly attributed to the slower aggregation rate but also related to the fact that light was more difficult to penetrate. However, for all tested concentrations, there was no significant aggregation in the nanosuspensions within 7000 s. Fig. 10c shows the variation of the transmitted light intensity over time from top to bottom of the sample. Even for the 0.005% sample with the largest TSI, the thickness of the color lines did not expand much, which meant that the intensity did not change significantly. The ripples of the curves at the top height may be due to the effects of gravity and van der Waals forces, which would drive the suspended nanosheets downward. The consequence could also be seen in Fig. 10d. As the concentration in the lower region increased,

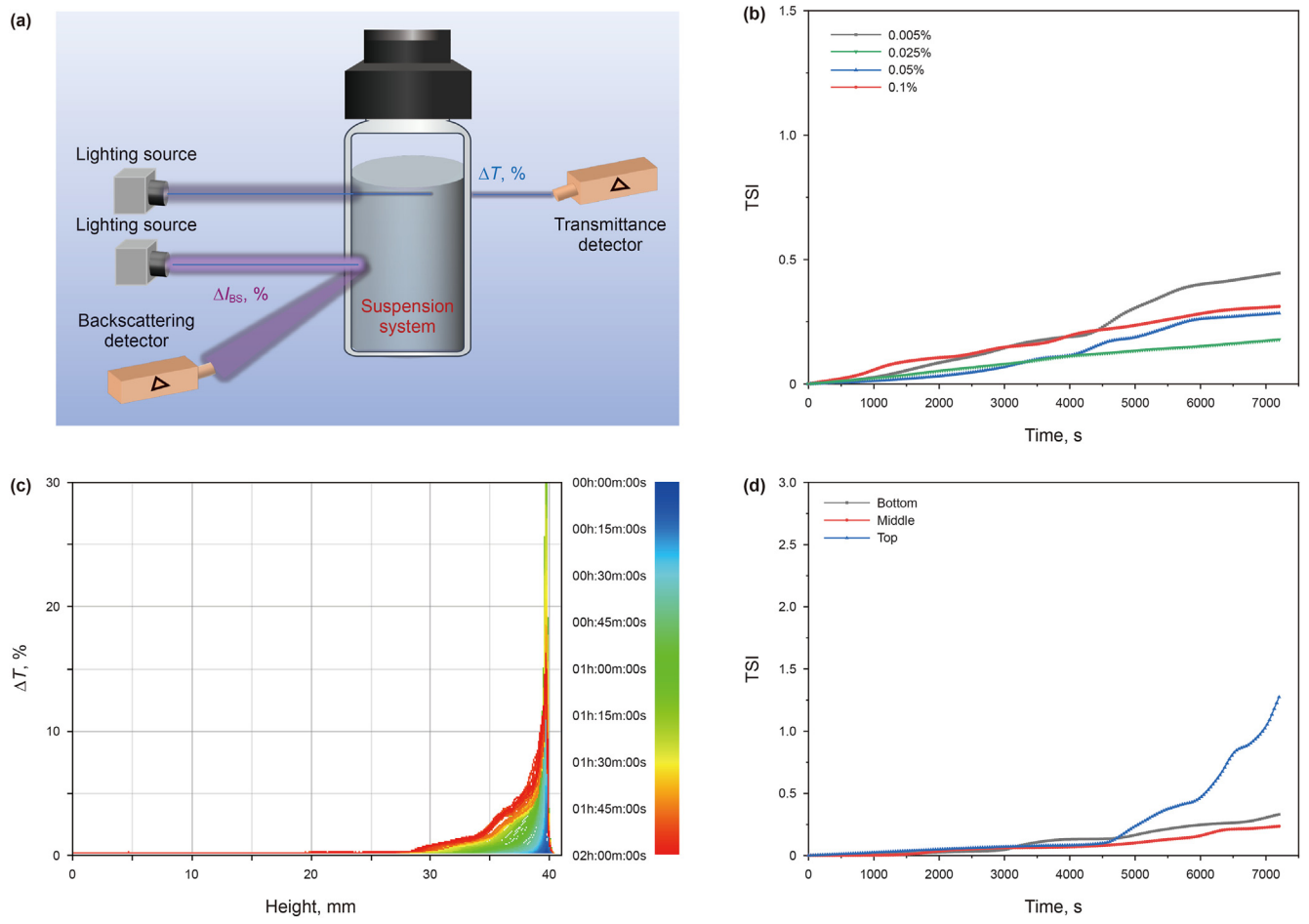

Fig. 10. (**a**) Schematic diagram of the Turbiscan device; **(b)** TSI of JAPNs with different concentrations; **(c)** The variation of the transmitted light intensity (ΔT)**; (d)** TSI of JAPNs (0.005%) at different heights.

the flexible polymer network and the surface polymer brush would spontaneously prevent further proximity between particles, which was known academically as steric hindrance stability.

3.3.3. Optical microrheology

The above dispersion experiments rely on the transmittance changes of the nanosuspension after a period of settlement, but the real migration state of the nanosheets at a certain moment remains unknown, which is also neglected in most past works. Herein, a new method called optical microrheology was pioneered to explore the dynamic movement process of nanosuspensions. It was not until 2012 that the Rheolaser optical microrheometer was marketed by the Formulaction Company. The Rheolaser equipment was mostly used to analyze the viscoelastic properties of soft substances, especially gels, in the past 10 years (Shen et al., 2021; Tisserand et al., 2012). However, based on the principle of multispeckle-DWS (MS-DWS), Rheolaser has the ability to qualitatively track the nanoscale motion behavior of dispersed particles (Shen et al., 2022). The schematic diagram is shown in Fig. 11a. When light shines on solid particles, a speckle pattern of backscattered light will be formed, which moves with the particles. The internal structural characteristics of the sample, namely the microscopic migration state of particles, can be characterized by the speed of speckle deformation (Zhang et al., 2016). Fig. 11b shows the mean square displacement (MSD) curves of JAPNs with decorrelation time. According to the slope of the curves, the MSD of JAPNs could be segmented into three stages. Since only when MSD curves are present as inclined ladder shapes, it means that the polymers have formed network gels in aqueous solution (Shen et al., 2021). However, almost all curves in area 3 are straight lines, and the MSD is proportional to the decorrelation time, which represents that the suspension system conforms to the characteristics of an ordinary viscous Newtonian fluid. The partial misalignment of color implied the inhomogeneity within the sample. Interestingly, there are two different areas early on. In area 1, the slope of the curve decreased near the middle. The disordered thermal motion of the suspended nanosheets causes squeezing and collision with other nanosheets, resulting in slower movement. However, due to the spatial effect of the polymer chain and the electrostatic repulsion of the hydrophilic groups, the suspension system would not undergo aggregation right away until about 8 h, as the line marked black. The slope of the curve decreases and then increases in area 2, which indicated that some nanosheets turn into ballistic motion after approaching. For this system, ballistic motion stands for settlement. Macroscopically, the initially homogeneous suspension starts to be unstable due to factors such as thermal motion, gravitational force, hydrophobic effect, and nano-effect. Even though it's not visible to the human eye, the nanosheets were detected to move downward through the unique mean of MS-DWS. The onset of the unstable phase used to be difficult to detect by conventional methods because the suspensions had no obvious change in appearance at this stage. The Tyndall phenomenon is still apparent and may become even more pronounced as the size of the aggregated particles becomes larger. In addition, the TSI analyzer is

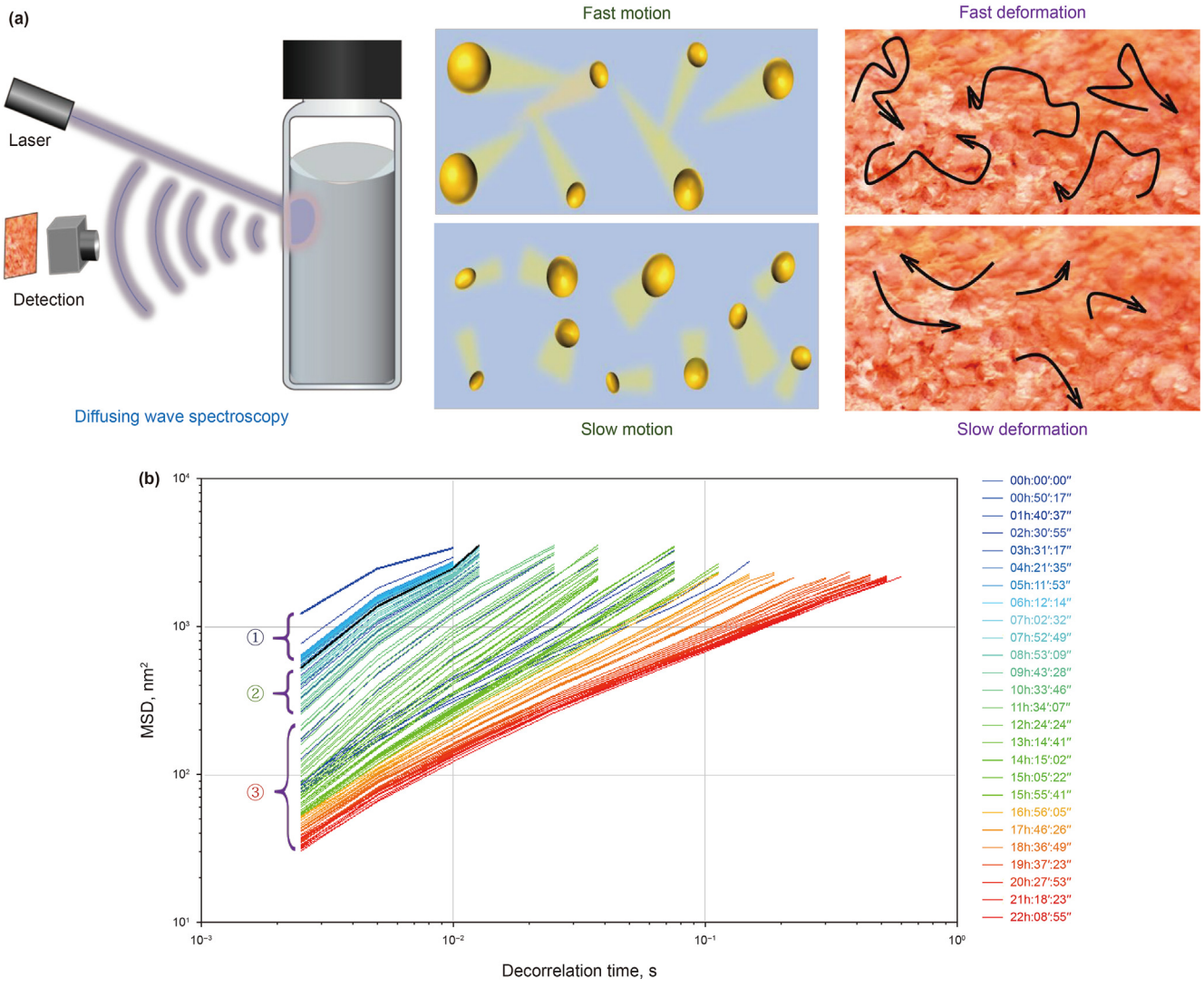

Fig. 11. (**a**) Schematic diagram of optical microrheology; **(b)** MSD curves of JAPNs with decorrelation time.

limited by its working mechanism, which is subject to the comprehensive analysis of the overall solution from top to bottom. To the best of our knowledge, the use of microrheology to determine the occurrence of substantial instability in nanosheet suspensions has not been used by other researchers. Through this attempt at cross-science combination, optical microrheology is expected to provide a new way of thinking for the stability analysis of nanosheet suspensions, as well as solid dispersion systems, which play an important role for their colloidal products in the storage, transportation, and application processes.

3.4. Interfacial properties

Interfacial adsorption refers to the enrichment of substances at the interface in order to reduce the free energy of the system. Because nanosheets are much larger than surfactant molecules, their ability to transport to the interface and reduce the IFT is weaker than that of common surfactants. It is necessary to study the interfacial properties of nanosheets under different conditions for guidance on EOR. Due to the amphiphilic Janus nature, AJNs are also known as "colloidal surfactants". Fig. 12a shows the ability of JAPNs to reduce the IFT of xylenes/brine and xylenes/brine/JAPNs. As a common nonpolar solvent containing three isomers, there was a large interfacial repulsion between xylenes and water. The IFT of xylenes/brine turned out to be about 35.6 mN/m. For the xylenes/brine/JAPNs system, as soon as the brine droplet was formed, the IFT started to decrease as the amphiphilic nanosheets adsorbed to the two-phase interface. In the early stage, the decline rate of IFT was faster. As the amphiphilic JAPNs adsorbed to the interface, the IFT gradually decreased to a relatively stable value, 19.72 mN/m. With the dual functionalities of IFT reduction and nanoparticles' Pickering effect, JAPNs could emulsify the xylene and water with the help of ultrasound. Fig. 12b shows the white emulsion of xylene/water/JAPNs and its optical microscope image. Studies have reported that the adsorption energy of Janus particles at the oil–water interface could be three times that of homogeneous particles (Binks and Fletcher, 2001). The interface stability of amphiphilic nanosheets will be further improved. Therefore, emulsion droplets will be more difficult to coalesce due to the protection of solid particle film on the surface. Compared to conventional surfactants, the ability of JAPNs to reduce IFT was inferior. Many studies had proved that one of the most important EOR mechanisms of amphiphilic nanosheets was to migrate to the oil–water–rock three-phase region, forming molecular deposition films and

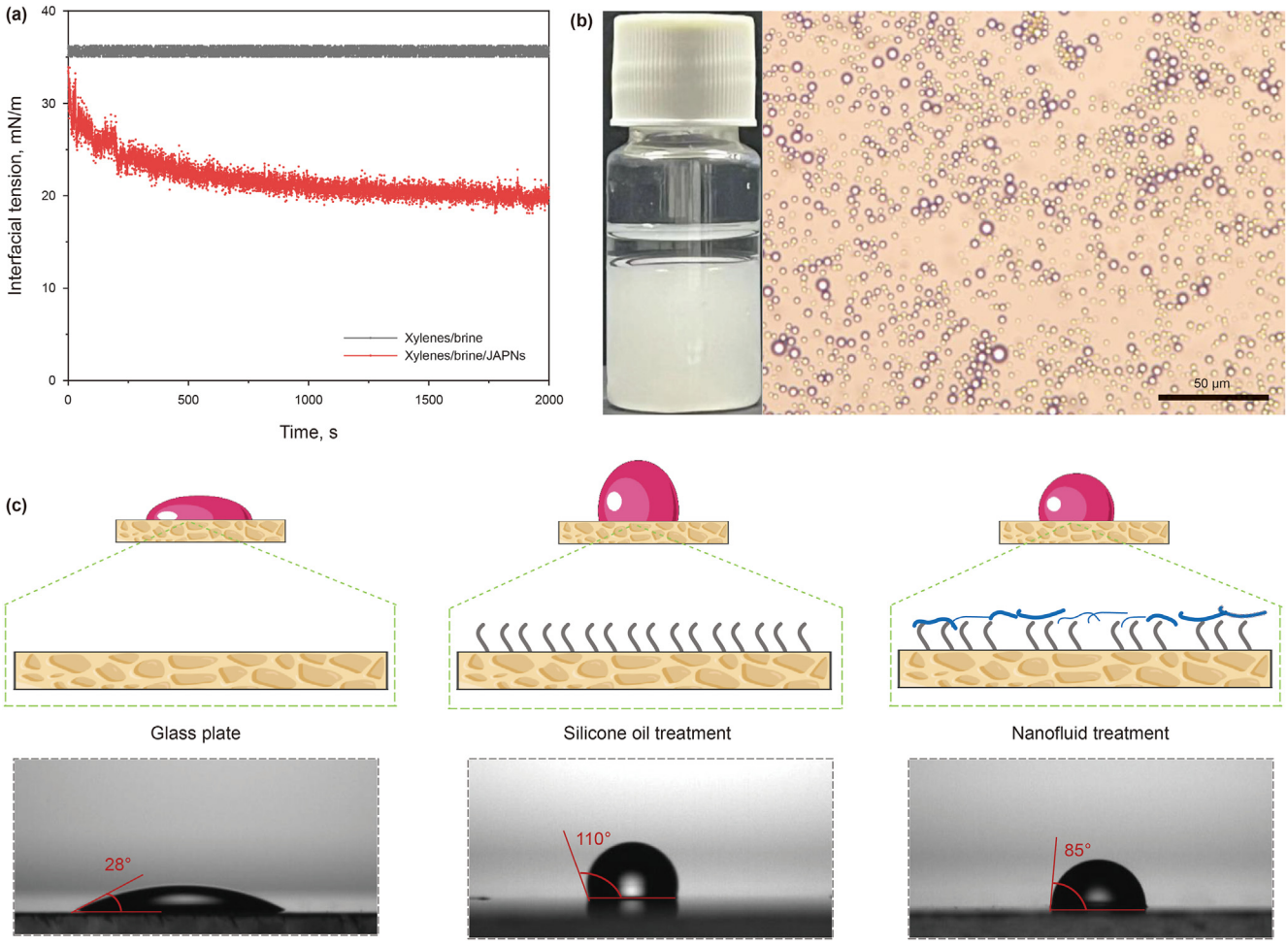

Fig. 12. (**a**) Dynamic interfacial tensions of xylenes/brine and xylenes/brine/JAPNs systems; **(b)** Emulsion formed by JAPNs and its optical microscope image; **(c)** Water contact angles of glass plates.

changing the wettability of the rock surface (Liang et al., 2022; Qu et al., 2020). The ability of JAPNs to change the wettability of glass flakes was shown in Fig. 12c. Glass flakes were soaked in silicone oil for 48 h to create oleophilic surfaces. Then they were transferred into JAPNs nanofluid for another 24 h. The initial contact angle of glass flakes was 28°. After being treated by the JAPNs nanofluid, the amphiphilic nanosheets could automatically adsorb to the surface. The oleophilic side of JAPNs faced the oil film and the hydrophilic groups pointed to the aqueous phase. A contact angle greater than 105° indicated that the surface was oil wetting, between 75° and 105° would be considered neutral wetting (Qu et al., 2021). Therefore, the surface wettability of the glass flakes was altered from oil wetting (110°) to neutral wetting (85°) by JAPNs nanofluids. The above experiments showed that the JAPNs had excellent dispersion stability and interfacial adsorption, which was positive for the application in EOR process.

3.5. EOR capacity

The physical properties and experimental conditions of the homogeneous cores are listed in Table 1. A relatively low concentration of nanofluids (0.005%) was chosen for nanoflooding experiments, which was in consideration of liquid density, materials cost, and reducing blocking. The injection performance of JAPNs was studied by comparing water and nanofluids injected at the same flow rate using the same unsaturated homogeneous core. As shown in Fig. 13a, the pressure difference of the water injection was stabilized at 218 kPa. After the JAPNs nanofluid was transferred, there was a gradual upward trend in pressure, which was related to the increase in fluid density and inhomogeneity, as well as the blockage of fine pores in the core by solid nanosheets. However, it was worth noting that even with 2.5 PV of nanofluid being injected, the pressure had only increased by 102 kPa. The improvement in injection performance could be attributed to two reasons. Firstly, the surface of the JAPNs contained abundant hydrophilic amino and carboxyl groups, which could improve their stability in aqueous solution. Therefore, they would not gather into large aggregates in advance in the storage tank and injection process, but could form uniform displacement fluid deep into the cores. Secondly, with the help of the flexible polymer framework of JAPNs, the 2D nanosheets could be curled or deformed to pass through the pore passages.

As for EOR experiments, reaction conditions of different aging times (0, 6, and 12 h) and two low permeability cores (2.5 and 25 mD) were examined. As shown in Fig. 13b and c, during the primary water flooding, the pressure increased in the early stages. Subsequently, as the oil in the core was continuously extracted, the injection pressure dropped accordingly and eventually leveled off due to the water breakthrough effect. In the process of nanofluid flooding, the pressure climbed up due to the temporary blocking of JAPNs in the areas with small pore throats. The increase of fluid

Table 1
Physical properties and experimental conditions.

Number	Length, mm	Diameter, mm	Real permeability, mD	Permeability specification, mD	Aging time, h	Total recovery, %
1	70.0	25.0	2.18	2.5	None	None
2	70.0	25.0	2.58	2.5	0	13.92
3	70.0	25.0	2.79	2.5	6	17.14
4	70.0	25.0	3.06	2.5	12	15.57
5	70.0	25.0	26.42	25	6	10.00

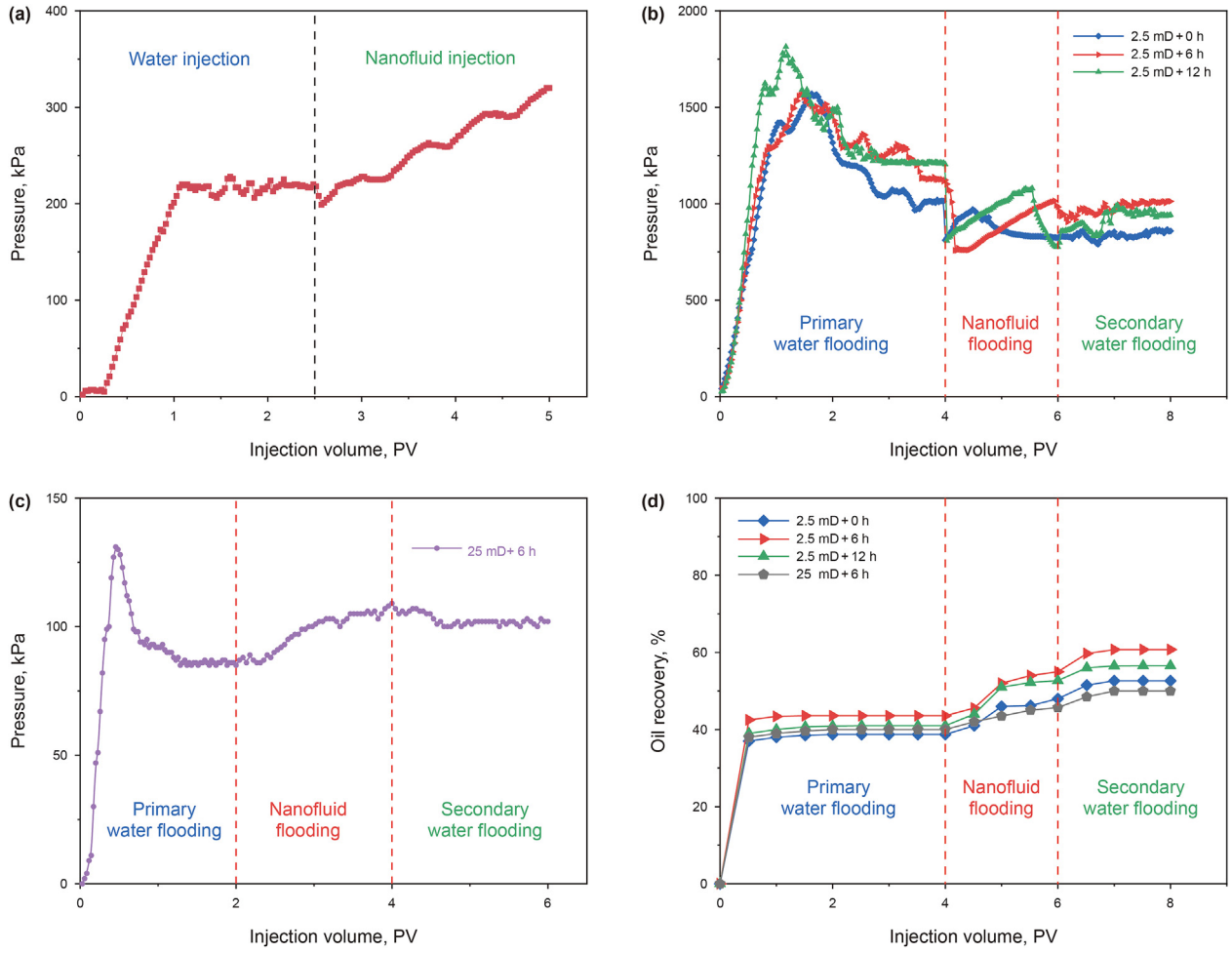

Fig. 13. (**a**) Injection performance experiment; (**b**, **c**) The pressure curves and (**d**) oil recovery curves during core displacements.

viscosity also contributed according to Darcy's formula. It is noted that, for the 2.5 mD cores, the pressure in the later stages of nanofluid flooding may drop down and even be lower than the equilibrium pressure of primary water flooding. The results may be explained that the JAPNs nanofluid could initiate residual oil that was difficult to be recovered in the primary water flooding, so that some pores in previously oil-bearing zones would also be unobstructed. Furthermore, since the amphiphilic nanosheets could change the wettability of rock and further wash off the residual oil, the capillary force of the core would be reduced. As the oil in the core had been driven out constantly, the residual pressure of the secondary water flooding would be lower than that of the primary water flooding. For core of higher permeability, the pressure during the whole displacement process was relatively low. The difference of stable pressure between primary and secondary water flooding could be attributed to the plugging of channeling pores by nanosheets. As shown in Fig. 13d, the oil recovery after aging for 6 h (17.14%) and 12 h (15.57%) was higher than that of the no-aging group (13.92%). Due to the slow injection rate and small core volume, 6 h had reached a suitable aging time for EOR. Driven by amphiphilic lamellar structure and nano-agglomeration effect, the nanosheets tended to adsorb in the three-phase region to form a wedge film. As the concentration of nanosheets in the wedge film increased, the resulting separation pressure would push the oil droplets forward. The specific surface area of the low permeability core was larger than that of the higher permeability core (10.00%), which provided more contact opportunities for the nanofluids and the crude oil adsorbed on the rock surface. The displacement experiments illustrated that the JAPNs nanofluid could enhance the recovery rate by 17.14% even under an ultra-low concentration of 0.005% and was more suitable for cores with relatively low permeability.

4. Summary and conclusions

In conclusion, we have introduced a type of organic-based, flexible, and high-performance JAPNs. The copolymer adsorption, amidation cross-linking, and denucleation were accomplished by melting, solidification, and dissolution processes of the phase change template. The lateral sizes of JAPNs were ranging from hundreds of nanometers to several micrometers and the thickness was about 3 nm. The flexible structure of the framework was beneficial for the injection performance of JAPNs nanofluids. The numerous amide, secondary amine, and carboxyl groups on the surface of the nanosheets not only enhance their hydrophilicity, but also provide active sites for further grafting modification. The JAPNs suspension exhibited good dispersion stability. The settling time with NaCl and $CaCl_2$ at a low salinity of 1000 mg/L was over 240 h. The value could also remain 124 h under the salinity of 10,000 mg/L NaCl. As an excellent "colloidal surfactant", JAPNs could change rock wettability, reduce IFT, and emulsify oil/water mixture. In particular, Rheolaser optical microrheology was developed to analyze the destability start-up state of nanosheet suspensions, which had not been reported by other researchers to our knowledge. In addition, the oil displacement experiments revealed that the JAPNs nanofluids could enhance recovery factor by 17.14%. The research on JAPNs offers new potential candidates as novel nanofluid agents for EOR application.

Based on the above results and discussion, the conclusions can be summarized as follows:

(1) A type of organic-based, flexible, and high-performance JAPNs was synthesized by paraffin emulsion methods. The copolymer adsorption, amidation cross-linking, and denucleation were accomplished by melting, solidification, and dissolution processes of the phase change template.
(2) Preliminary characterization of JAPNs was studied systematically. The lateral sizes were ranging from hundreds of nanometers to several micrometers and the thickness was about 3 nm. The flexible structure of the framework was beneficial for the injection performance of JAPNs nanofluids. The numerous amide, secondary amine, and carboxyl groups on the surface of the nanosheets not only enhance their hydrophilicity, but also provide active sites for further grafting modification.
(3) Compared with traditional types of AJNs, JAPNs suspension exhibited good dispersion stability. The settling time with NaCl and $CaCl_2$ at a low salinity of 1000 mg/L was over 240 h. The value could also remain 124 h under the salinity of 10,000 mg/L NaCl.
(4) As sedimentation lagges behind aggregation, it is difficult to accurately detect the onset time of the decreasing effectiveness for nanofluid products. Herein, Rheolaser optical microrheology was developed to analyze the destability start-up state of nanosheet suspensions, which had not been reported by other researchers to our knowledge.
(5) As an excellent "colloidal surfactant", JAPNs could change rock wettability, reduce IFT, and emulsify oil/water mixture. The oil displacement experiments revealed that the JAPNs nanofluids could enhance recovery factor by 17.14%. The research on JAPNs offers new potential candidates as novel nanofluid agents for EOR application.

Declaration of competing interest

The authors declare that they have no known competing financial interests or personal relationships that could have appeared to influence the work reported in this paper.

Acknowledgements

This research was supported by the National Natural Science Foundation of China (52074320) and Petrochina Strategic Cooperation Science and Technology Project (ZLZX2020-01-04-03). We also thank the Institute of Chemistry Chinese Academy of Sciences for their academic assistance.

References

Binks, B.P., Fletcher, P., 2001. Particles adsorbed at the oil–water interface: a theoretical comparison between spheres of uniform wettability and "Janus" particles. Langmuir 17 (16), 4708–4710. https://doi.org/10.1021/la0103315.
Chen, Y., Liang, F., Yang, H., Zhang, C., Wang, Q., Qu, X., Li, J., Cai, Y., Qiu, D., Yang, Z., 2012. Janus nanosheets of polymer–inorganic layered composites. Macromolecules 45 (3), 1460–1467. https://doi.org/10.1021/ma2021908.
Haruna, M.A., Wen, D., 2019. Stabilization of polymer nanocomposites in high-temperature and high-salinity brines. ACS Omega 4 (7), 11631–11641. https://doi.org/10.1021/acsomega.9b00963.
Hua, Z., Tang, Z., Bai, X., Zhang, J., Yu, L., Cheng, H., 2015. Aggregation and resuspension of graphene oxide in simulated natural surface aquatic environments. Environ. Pollut. 205, 161–169. https://doi.org/10.1016/j.envpol.2015.05.039.
Jin, Z., Wang, Y., Liu, J., Yang, Z., 2008. Synthesis and properties of paraffin capsules as phase change materials. Polymer 49 (12), 2903–2910. https://doi.org/10.1016/j.polymer.2008.04.030.
Ke, H., Yuan, M., Xia, S., 2022. A review of nanomaterials as viscosity reducer for heavy oil. J. Dispersion Sci. Technol. 43 (9), 1271–1282. https://doi.org/10.1080/01932691.2020.1851246.
Li, Z., Wu, H., Yang, M., Xu, D., Chen, J., Feng, H., Lu, Y., Zhang, L., Yu, Y., Kang, W., 2017. Stability mechanism of o/w Pickering emulsions stabilized with regenerated cellulose. Carbohydr. Polym. 224–233. https://doi.org/10.1016/j.carbpol.2017.10.080.
Liang, F., Shen, K., Qu, X., Zhang, C., Wang, Q., Li, J., Liu, J., Yang, Z., 2011. Inorganic Janus nanosheets. Angew. Chem., Int. Ed. 50 (10), 2379–2382. https://doi.org/10.1002/anie.201007519.
Liang, F., Liu, B., Cao, Z., Yang, Z., 2018. Janus colloids toward interfacial engineering. Langmuir 34 (14), 4123–4131. https://doi.org/10.1021/acs.langmuir.7b02308.
Liang, T., Hou, J., Qu, M., Xi, J., Raj, I., 2022. Application of nanomaterial for enhanced oil recovery. Petrol. Sci. 19 (2), 882–899. https://doi.org/10.1016/j.petsci.2021.11.011.
Liu, Y., Xu, X., Liang, F., Yang, Z., 2017. Polymeric Janus nanosheets by template raft polymerization. Macromolecules 50 (22), 9042–9047. https://doi.org/10.1021/acs.macromol.7b01558.
Luo, D., Wang, F., Alam, M.K., Yu, F., Mishra, I.K., Bao, J., Willson, R.C., Ren, Z., 2017. Colloidal stability of graphene-based amphiphilic Janus nanosheet fluid. Chem. Mater. 29 (8), 3454–3460. https://doi.org/10.1021/acs.chemmater.6b05148.
Luo, D., Wang, F., Chen, J., Zhang, F., Yu, L., Wang, D., Willson, R.C., Yang, Z., Ren, Z., 2018. Poly(sodium 4-styrenesulfonate) stabilized Janus nanosheets in brine with retained amphiphilicity. Langmuir 34 (12), 3694–3700. https://doi.org/10.1021/acs.langmuir.8b00397.
Luo, D., Zhang, F., Ding, F., Ren, B., Ren, Z., 2019. Interactions between amphiphilic Janus nanosheets and a nonionic polymer in aqueous and biphasic systems. Soft Matter 15 (37), 7472–7478. https://doi.org/10.1039/C9SM00994A.
Lv, Q., Zheng, R., Zhou, T., Guo, X., Wang, W., Li, J., Liu, Z., 2022. Visualization study of CO_2-EOR in carbonate reservoirs using 2.5D heterogeneous micromodels for CCUS. Fuel 330, 125533. https://doi.org/10.1016/j.fuel.2022.125533.
McClements, D.J., 2005. Theoretical analysis of factors affecting the formation and stability of multilayered colloidal dispersions. Langmuir 21 (21), 9777–9785. https://doi.org/10.1021/la0512603.
Mu, L., Yang, S., Hao, B., Ma, P., 2015. Ternary silicone sponge with enhanced mechanical properties for oil–water separation. Polym. Chem. 6 (32), 5869–5875. https://doi.org/10.1039/C5PY00861A.
Olayiwola, S.O., Dejam, M., 2021. Comprehensive experimental study on the effect of silica nanoparticles on the oil recovery during alternating injection with low salinity water and surfactant into carbonate reservoirs. J. Mol. Liq. 325, 115178. https://doi.org/10.1016/j.molliq.2020.115178.
Peplow, M., 2016. The plastics revolution: how chemists are pushing polymers to new limits. Nature 536 (7616), 266–268. https://doi.org/10.1038/536266a.
Percebom, A.M., Costa, L.H.M., 2019. Formation and assembly of amphiphilic Janus nanoparticles promoted by polymer interactions. Adv. Colloid Interfac. 269, 256–269. https://doi.org/10.1016/j.cis.2019.05.001.
Qu, M., Hou, J., Liang, T., Xiao, L., Yang, J., Raj, I., Shao, Y., 2020. Preparation and interfacial properties of ultralow concentrations of amphiphilic molybdenum disulfide nanosheets. Ind. Eng. Chem. Res. 59 (19), 9066–9075. https://doi.org/10.1021/acs.iecr.0c00217.
Qu, M., Hou, J., Liang, T., Qi, P., 2021. Amphiphilic rhamnolipid molybdenum disulfide nanosheets for oil recovery. ACS Appl. Nano Mater. 4 (3), 2963–2972. https://doi.org/10.1021/acsanm.1c00102.
Qu, M., Liang, T., Xiao, L., Hou, J., Qi, P., Zhao, Y., Song, C., Li, J., 2022a. Mechanism study of spontaneous imbibition with lower-phase nano-emulsion in tight reservoirs. J. Petrol. Sci. Eng. 211, 110220. https://doi.org/10.1016/j.petrol.2022.110220.

Qu, M., Liang, T., Hou, J., Liu, Z., Yang, E., Liu, X., 2022b. Laboratory study and field application of amphiphilic molybdenum disulfide nanosheets for enhanced oil recovery. J. Petrol. Sci. Eng. 208, 109695. https://doi.org/10.1016/j.petrol.2021.109695.

Rezk, M.Y., Allam, N.K., 2019. Impact of nanotechnology on enhanced oil recovery: a mini-review. Ind. Eng. Chem. Res. 58 (36), 16287–16295. https://doi.org/10.1021/acs.iecr.9b03693.

Scheirs, J., Priddy, D.B., 2003. Modern Styrenic Polymers: Polystyrenes and Styrenic Copolymers. Wiley. https://doi.org/10.1002/0470867213.

Shen, H., Yang, Z., Li, X., Peng, Y., Lin, M., Zhang, J., Dong, Z., 2021. CO_2-responsive agent for restraining gas channeling during CO_2 flooding in low permeability reservoirs. Fuel 292, 120306. https://doi.org/10.1016/j.fuel.2021.120306.

Shen, H., Yang, Z., Xiong, Y., Cao, Q., Xu, K., Lin, M., Zhang, J., Dong, Z., 2022. An organic-based amphiphilic Janus polymer nanosheet: synthesis, properties, and microscopic dispersion interpretations. J. Mol. Liq. 363, 119822. https://doi.org/10.1016/j.molliq.2022.119822.

Stupp, S.I., Son, S., Li, L.S., Lin, H.C., Keser, M., 1995. Bulk synthesis of two-dimensional polymers: the molecular recognition approach. J. Am. Chem. Soc. 117 (19), 5212–5227. https://doi.org/10.1021/ja00124a005.

Tan, C., Cao, X., Wu, X.J., He, Q., Yang, J., Zhang, X., Chen, J., Zhao, W., Han, S., Nam, G.H., 2017. Recent advances in ultrathin two-dimensional nanomaterials. Chem. Rev. 6225. https://doi.org/10.1021/acs.chemrev.6b00558.

Tisserand, C., Fleury, M., Brunel, L., Bru, P., Meunier, G., 2012. Passive Microrheology for Measurement of the Concentrated Dispersions Stability. Springer Berlin Heidelberg. https://doi.org/10.1007/978-3-642-28974-3_17.

Walther, A., Müller, A.H.E., 2008. Janus particles. Soft Matter 4 (4), 663. https://doi.org/10.1039/b718131k.

Wasan, D.T., Nikolov, A.D., 2003. Spreading of nanofluids on solids. Nature 423 (6936), 156–159. https://doi.org/10.1038/nature01591.

Xiong, R., Guo, J., Kiyingi, W., Feng, H., Sun, T., Yang, X., Li, Q., 2020. Method for judging the stability of asphaltenes in crude oil. ACS Omega 5 (34), 21420–21427. https://doi.org/10.1021/acsomega.0c01779.

Xue, Z., Foster, E., Wang, Y., Nayak, S., Cheng, V., Ngo, V.W., Pennell, K.D., Bielawski, C.W., Johnston, K.P., 2014. Effect of grafted copolymer composition on iron oxide nanoparticle stability and transport in porous media at high salinity. Energy Fuel. 28 (6), 3655–3665. https://doi.org/10.1021/ef500340h.

Yakasai, F., Jaafar, M.Z., Bandyopadhyay, S., Agi, A., 2021. Current developments and future outlook in nanofluid flooding: a comprehensive review of various parameters influencing oil recovery mechanisms. J. Ind. Eng. Chem. 93, 138–162. https://doi.org/10.1016/j.jiec.2020.10.017.

Yin, T., Yang, Z., Lin, M., Zhang, J., Dong, Z., 2019a. Aggregation kinetics and colloidal stability of amphiphilic Janus nanosheets in aqueous solution. Ind. Eng. Chem. Res. 58 (11), 4479–4486. https://doi.org/10.1021/acs.iecr.8b06413.

Yin, T., Yang, Z., Lin, M., Zhang, J., Dong, Z., 2019b. Preparation of Janus nanosheets via reusable cross-linked polymer microspheres template. Chem. Eng. J. 371, 507–515. https://doi.org/10.1016/j.cej.2019.04.093.

Yin, T., Yang, Z., Dong, Z., Lin, M., Zhang, J., 2019c. Physicochemical properties and potential applications of silica-based amphiphilic Janus nanosheets for enhanced oil recovery. Fuel 237, 344–351. https://doi.org/10.1016/j.fuel.2018.10.028.

Yin, T., Yang, Z., Zhang, F., Lin, M., Zhang, J., Dong, Z., 2020. Probing the impact of surface chemistry on the microscopic interactions between amphiphilic Janus nanosheets and water. Ind. Eng. Chem. Res. 59 (32), 14344–14351. https://doi.org/10.1021/acs.iecr.0c02249.

Yin, T., Yang, Z., Zhang, F., Lin, M., Zhang, J., Dong, Z., 2021. Assembly and mechanical response of amphiphilic Janus nanosheets at oil-water interfaces. J. Colloid Interface Sci. 583, 214–221. https://doi.org/10.1016/j.jcis.2020.09.026.

Zeng, Y., Gordiichuk, P., Ichihara, T., Zhang, G., Sandoz-Rosado, E., Wetzel, E.D., Tresback, J., Yang, J., Kozawa, D., Yang, Z., Kuehne, M., Quien, M., Yuan, Z., Gong, X., He, G., Lundberg, D.J., Liu, P., Liu, A.T., Yang, J.F., Kulik, H.J., Strano, M.S., 2022. Irreversible synthesis of an ultrastrong two-dimensional polymeric material. Nature 602 (7895), 91–95. https://doi.org/10.1038/s41586-021-04296-3.

Zhan, G., Cai, Z., Strutyński, K., Yu, L., Herrmann, N., Martínez-Abadía, M., Melle-Franco, M., Mateo-Alonso, A., Feyter, S.D., 2022. Observing polymerization in 2D dynamic covalent polymers. Nature 603 (7903), 835–840. https://doi.org/10.1038/s41586-022-04409-6.

Zhang, C., Liang, F., Yang, Z., 2018. Design, Synthesis, and Application of Anisotropic Janus Particles. World Scientific, pp. 1–30. https://doi.org/10.1142/9781786343130_000.

Zhang, F., Yang, Z., Yin, T., Li, X., Lin, M., Zhang, J., Dong, Z., 2022a. Simple and facile synthesis of magnetic nanosheets by improved precipitation method. J. Alloys Compd. 922, 166305. https://doi.org/10.1016/j.jallcom.2022.166305.

Zhang, F., Yang, Z., Yin, T., Shen, H., Liang, W., Li, X., Lin, M., Zhang, J., Dong, Z., 2022b. Study of Pickering emulsions stabilized by Janus magnetic nanosheets. Colloid. Surface. 654, 130194. https://doi.org/10.1016/j.colsurfa.2022.130194.

Zhang, Y., Kong, X., Gao, L., Lu, Z., Zhou, S., Dong, B., Xing, F., 2016. In-situ measurement of viscoelastic properties of fresh cement paste by a microrheology analyzer. Cement Concr. Res. 79, 291–300. https://doi.org/10.1016/j.cemconres.2015.09.020.

Zhou, P., Wang, Q., Zhang, C., Liang, F., Qu, X., Li, J., Yang, Z., 2015. pH responsive Janus polymeric nanosheets. Chin. Chem. Lett. 26 (6), 657–661. https://doi.org/10.1016/j.cclet.2015.04.006.